





Capacity, damage and fragility models for steel buildings: a probabilistic approach

Sergio A. Díaz^{1,3}  · Luis G. Pujades¹  · Alex H. Barbat² 
Diego A. Hidalgo-Leiva¹  · Yeudy F. Vargas-Alzate¹

Received: 14 December 2016 / Accepted: 12 September 2017 / Published online: 9 October 2017
© Springer Science+Business Media B.V. 2017

Abstract Recently proposed capacity-based damage indices and parametric models for capacity curves are applied to frame steel buildings located in soft soils of the Mexico City. To do that, the seismic performance of 2D models of low-, mid- and high-rise buildings is assessed. Deterministic and probabilistic nonlinear static and incremental dynamic analyses are implemented. Monte Carlo simulations and the Latin Hypercube sampling technique are used. Seismic actions are selected among accelerograms recorded in the study area. Spectral matching techniques are applied, so that the acceleration time histories have a predefined mean response spectrum and controlled error. The design spectrum of the Mexican seismic code for the zone is used as target spectrum. The well-known Park and Ang damage index allows calibrating the capacity-based damage index. Both damage indices take into account the contribution to damage of the stiffness degradation and of the energy dissipation. Damage states and fragility curves are also obtained and discussed in detail. The results reveal the versatility, robustness and reliability of the parametric model for capacity curves, which allow modelling the nonlinear part of the capacity curves by the cumulative integral of a cumulative lognormal function. However, these new capacity-based damage index and capacity models have been tested for and applied to 2D frame buildings only; they have not been applied to 3D building models yet. The Park and Ang and the capacity-based damage indices show that for the analysed buildings, the contribution to damage of the stiffness degradation is in the range 66–77% and that of energy loss is in the range 29–34%. The lowest contribution of energy dissipation (29%) is found for the low-rise, more rigid, building. The energy contribution would raise with the ductility of the building and with the duration of the strong ground motion. High-rise frame

✉ Sergio A. Díaz
sergio.alberto.diaz@upc.edu

¹ Polytechnic University of Catalonia, DECA-ETCG Barcelona Tech, Jordi Girona 1-3, 08034 Barcelona, Spain

² Polytechnic University of Catalonia, DECA-MMCE Barcelona Tech, Jordi Girona 1-3, 08034 Barcelona, Spain

³ Universidad Juárez Autónoma de Tabasco (UJAT), DAIA, Cunduacán, Tabasco, Mexico

buildings in soft soils of Mexico City show the worst performance so that the use of adequate braced frames to control the displacements could be recommended.

Keywords Non-linear structural analysis · Parametric model · Monte Carlo simulation · Steel buildings · Damage assessment

1 Introduction

The main purpose of this paper is to check the new damage index and the new capacity and fragility models, proposed by Pujades et al. (2015), when they are applied to steel buildings. In fact, this damage index and these parametric and fragility models have been tested only in a single simple reinforced concrete building; thus, the results of this paper will endorse the robustness, reliability and utility of these recent developments. Also, an important goal is to carry out a full probabilistic assessment of the seismic performance of low-, mid- and high-rise frame steel buildings in Mexico City. The method used by Vargas et al. (2013) to assess the seismic performance of a Reinforced Concrete (RC) building has been adopted; due to the regularity in plan and elevation, buildings are modelled as 2D frame structures in these works; applications to 3D building models await further research.

Concerning the new capacity model, the parametric model assumes that capacity curves are composed of a linear and a non-linear part. The linear part is defined by the initial stiffness or, equivalently, by a straight line whose slope (m) is defined by the fundamental period of vibration of the building. The non-linear part represents the degradation of the building and can be parameterized by means of the cumulative integral of a cumulative lognormal function and, therefore, it can be defined by two parameters, μ and σ ; the ultimate capacity point (the ultimate base shear, V_u , and the ultimate roof displacement, δ_u , in the capacity curve, or their corresponding, the ultimate spectral acceleration, Sa_u , and the ultimate spectral displacement, Sd_u , in the capacity spectrum) provides the two last parameters of the five fully defining the capacity curve. Figure 1 shows an example of a capacity curve defined by these five parameters. The first derivative of the non-linear part of the capacity curve is also shown in this figure. This first derivative displays the cumulative lognormal function.

Concerning the new damage index and fragility model, on the basis of damage observations, many damage indices have been published that can be used to assess expected damage in buildings affected by earthquakes. These damage indices are related to degradation of the overall capacity of the structure to withstand the foreseen seismic loads, and they are usually defined on the basis of variation of specific parameters representing the strength and/or weakness of the building. Thus, for instance, damage indices based on

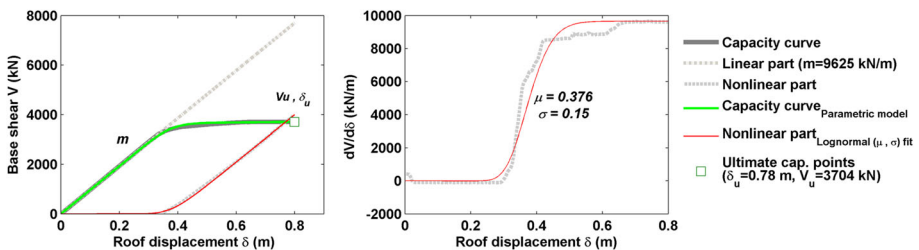


Fig. 1 Capacity curve as defined by five independent parameters

displacement ductility were used by Powell and Allahabadi (1988) and by Cosenza et al. (1993). Bracci et al. (1989) and Bojorquez et al. (2010) focused on energy dissipation; Krawinkler and Zohrei (1983) paid attention to cyclic fatigue. Changes (increases) in the natural period of the structure have also been used as damage indicators (DiPasquale and Cakmak 1990); Kamaris et al. (2013) focused on strength and stiffness degradation. Other authors, such as Banon and Veneziano (1982), Park and Ang (1985), Roufaiel and Meyer (1987) and Bozorgnia and Bertero (2001), connected the expected damage to combinations of the above parameters. Park and Ang or similar damage indices have been widely used to assess the seismic performance of steel buildings in recent studies; see, for instance, Barbosa et al. (2017); Liu et al. (2017), Zhou et al. (2016), Brando et al. (2015); Rajeev and Wijesundara (2014) and Levy and Lavan (2006). All these indices should be considered damage pointers and properly fulfil the purpose for which they were developed. However, in many cases, their calculation in practical applications involves Non Linear Dynamic Analysis (NLDA), which has high computational costs. More recently, a new capacity-based damage index was proposed by Pujades et al. (2015). This new damage index, which is based on secant stiffness degradation and energy dissipation, was successfully calibrated using a 2D model of a reinforced concrete frame buildings in such a way that it is equivalent to the well-known Park and Ang damage index (Park et al. 1985; Park and Ang 1985) obtained by means of NLDA. The main advantage of the new index is that, once calibrated, it can be obtained in an easy and straightforward way, directly from capacity curves.

Concerning the probabilistic assessment of the seismic performance of frame steel buildings in Mexico City, it is well known that variables involved in the seismic assessment of structures have high uncertainties. These uncertainties can be organized into aleatory (or random) and epistemic (or knowledge) uncertainties (Wen et al. 2003; McGuire 2004; Barbat et al. 2011). Epistemic uncertainties are due to lack of knowledge about models and/or parameters; aleatory uncertainty is inherent to random phenomena. Uncertainties in the seismic actions and in the properties of the buildings are considered. In relation to seismic actions, aleatory uncertainties are associated with the expected ground motions, and, therefore, they cannot be controlled, but they can be estimated and addressed through probabilistic approaches. In this research, uncertainties in seismic actions are defined by means of a suite of accelerograms whose acceleration response spectra have predefined mean and SD; the design spectra for soft soils in the city of Mexico (NTC-DF 2004) define the mean response spectrum. Regarding structures, aleatory uncertainties are due to unawareness of the precise mechanical and geometrical properties. Certainly, uncertainties in mechanical properties can be reduced by means of lab tests; in this research, the uncertainty model used by Kazantzi et al. (2014) has been adopted; thus, the mass, damping and other geometrical parameters are assumed to be deterministic, and the strength and ductility of structural elements are considered in a probabilistic way.

Another important issue is how uncertainties propagate. Because of non-linearity, uncertainties in the response strongly depend on the non-linear relations between inputs and outputs. Thus, to take into account the effect of uncertainties in the response, in deterministic approaches, seismic design standards recommend the use of reduced values for strength of materials and increased actions, by means of safety factors. However, in non-linear systems, it is well-known that the confidence levels associated with the response may be different from those associated with the input variables (Vargas et al. 2013). Thus, in the last two decades, the importance of performing probabilistic non-linear static analysis (NLSA) (ATC-40 1996; Freeman 1998) and non-linear dynamic analysis (NLDA) has been emphasized, (McGuire 2004) and, currently, there is a consensus that probabilistic approaches are more suitable than deterministic ones, as they allow the

incorporation of uncertainties, including confidence intervals, and thus provide more reliable results. However, NLDA is assumed to be the most appropriate method for assessing expected damage in structures subjected to dynamic actions (Vamvatsikos and Cornell 2002). Thus, when the capacity spectrum method (CSM) is used, it should be verified that the results are consistent with those obtained from Nonlinear Incremental Dynamic Analysis (NLIDA) (Mwafy and Elnashai 2001; Kim and Kurama 2008). In recent studies, probabilistic static and dynamic approaches have been implemented using the Monte Carlo simulation method (Fragiadakis and Vamvatsikos 2008, 2010; Vargas et al. 2013; Kazantzi et al. 2014; Barbat et al. 2016). But, probabilistic analyses require a significant number of NLIDAs and/or NLSAs, entailing a high computational cost. Therefore, it would be useful to take advantage of simplified methods to compare the results obtained by means of NLSA and NLIDA. An example of such a simplified approach is that proposed by Pujades et al. (2015).

In this research, both static and dynamic analyses are performed by means of a probabilistic approach that uses the Monte Carlo simulation method and the Latin Hypercube Sampling (LHS) technique to optimize the number of samples. This fully probabilistic approach can quantify the expected uncertainties in the response and in the expected damage, produced by uncertainties in the material properties and the seismic actions. The results show how uncertainties in the response and in the expected damage increase with the severity of seismic actions. Moreover, it is shown how, static and dynamic approaches provide consistent results. However, for the buildings analysed in this work, the consistency is lower for high-rise buildings. This fact is attributed to the likely influence of higher modes, which are not considered in the static analyses, as adopted herein. Finally, it is also shown that the capacity parametric model and capacity based damage index also hold for steel structures, so capacity curves can be represented by means of a simple model. The expected damage and fragility curves can be analysed directly from capacity curves, in a simple and straightforward way, thus avoiding the large amounts of computation involved in dynamic simulations.

2 Buildings

2.1 Structural models

Three steel buildings are analysed in this paper; namely high- (13 stories), mid- (7 stories) and low-rise (3 stories) buildings, with Special Moment Frames (SMF). Steel W type sections (wide flange American section) are used for beams and columns, which are joined by means of prequalified connections (ANSI/AISC 358-10 2010) of Fully Restrained (FR) type. Buildings were designed as offices, on the basis of the provisions for the México City area of NTC-DF (2004) and AISC-341-10 (2010) seismic codes. Buildings have rectangular floors, 3 beams of 5 m, in the transverse direction, and 4 beams of 6 m in the longitudinal direction. For each building, our focus will be on the central frame in the longitudinal direction. Buckling of columns was controlled in the analysis. The design of the SMFs satisfies the AISC criterion “strong- column-weak-beam” and the structural sections of the columns meet the slenderness criterion of the AISC-341-10 (2010). Figure 2 shows a sketch of the three 2D-models (SMF 3, SMF 7 and SMF 13).

NLSAs and NLIDAs were performed with Ruaumoko 2D software (Carr 2002). The weight of the structure, as well as that of the architectural finishes and facilities, were considered dead loads (DL), while live loads (LL) were established according to NTC-DF (2004) provisions for office use. Total gravity loads for non-linear analysis are established

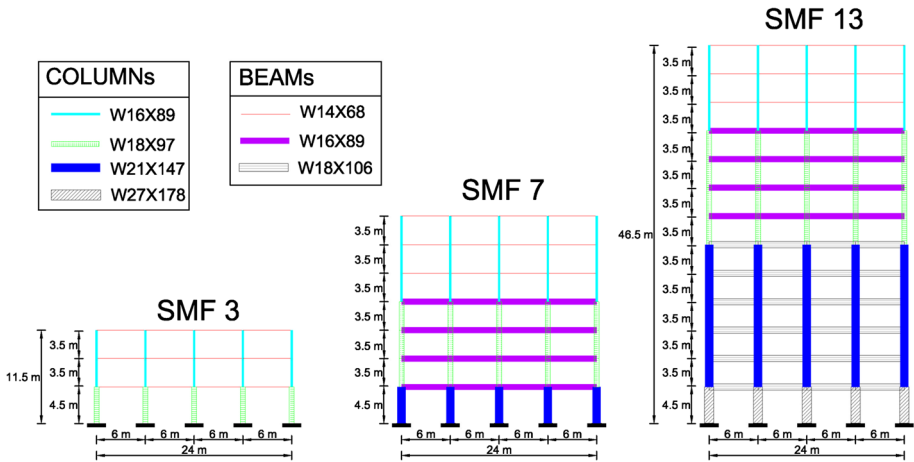


Fig. 2 2D building models

as 1.0 DL + 0.2 LL (PEER/ATC 72-1 2010). Beams and columns were modelled as FRAME type members, with plastic hinges at their ends. Plastic hinges follow the Bi-Linear Hysteresis rule, with hardening and strength reduction based on the ductility factor [see Appendix A—Ruaumoko 2D (Carr 2002)]. For columns, the plastic surface is defined by means of the interaction diagram relating the bending moment and the axial force. For beams, the yielding surface is defined by means of the curve relating the bending moment to the rotation. Moreover, the values of strength and ductility for the hysteresis rule were calculated according to the modified Ibarra–Medina–Krawinkler (IMK) model (Ibarra et al. 2005; Lignos and Krawinkler 2011, 2012, 2013). This model establishes strength bounds on the basis of a monotonic backbone curve (Fig. 3a). The backbone curve is defined by three strength parameters (M_y = effective yield moment, M_c = capping moment strength—or post-yield strength ratio M_c/M_y —and $M_r = \kappa \cdot M_y$, $\kappa = 0.4$, residual moment) and by four deformation parameters (θ_y = yield rotation, θ_p = pre-capping plastic rotation for monotonic loading—difference between yield rotation and rotation at maximum moment, θ_{pc} = post-capping plastic rotation—difference between rotation at maximum moment and rotation at complete loss of strength—and θ_u = ultimate rotation capacity) (Lignos and Krawinkler 2011). The columns of the moment-resisting bays were assumed to be fixed at their bases. P-Delta effects have been considered in all the simulations to take into account the global stability of the structure. The panel zones were

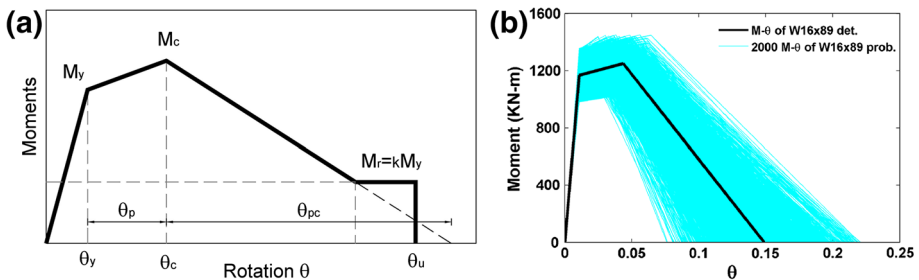


Fig. 3 **a** Modified IMK model: monotonic curve; **b** M– θ diagrams for the pure bending case 200 random simulations for each one of the 10 columns type W16x89 are plotted

modelled by the rotational stiffness in the connections, obtained according to the model proposed by Krawinkler (1978) and presented in FEMA 355C (2000). In all cases, as recommended for steel structures, for the first and last vibration mode under consideration (SAC 1996), 2% Rayleigh damping was assumed. The fundamental periods of the models are 0.632, 1.22 and 1.92 s for SMF3, SMF7 and SMF13 buildings respectively.

2.2 Probabilistic variables

There are many sources of uncertainties in structural analysis. Even geometric properties, such as thickness, length and width of the structural elements or of the structure itself, can be considered probabilistic variables. Concerning mechanical properties, several parameters can be considered in a probabilistic way, such as Young’s modulus, ultimate strength, plastic modulus and so on. However, to make the probabilistic approach clearer and easier, in this study only a few properties are considered in a probabilistic manner. Thus, the probabilistic model for mechanical properties used by Kazantzi et al. (2014) has been adopted so that only uncertainties in strength and ductility are considered. In order to see the influence of uncertainties in mechanical properties on uncertainties in the response, an uncertainty analysis will also be performed. This analysis will show how the most important source of uncertainty is that due to seismic actions, although that due to mechanical properties may also be significant. Thus, in this study, the mass, damping and other geometrical parameters are assumed deterministic, and the strength and ductility of structural elements are considered in a probabilistic way.

Concerning strength, all the parameters of the modified IMK model can be obtained from three properties of the sections. That is, plastic modulus, Z , expected yield strength, f_y , and modulus of elasticity, E . Moreover, due to the fact that E and Z , for W sections, have low coefficients of variation (COV), and taking into account that E is directly related to f_y by means of the strain ϵ_y , whose value for steel is accurately determined, it is considered that uncertainty in f_y can take up the low uncertainties of E and Z , thus avoiding overestimations of uncertainties in the strength parameters. Notably, COV takes values between 1 and 3% (Bartlett et al. 2003) for E , and between 1 and 2% (Jaquess and Frank 1999; Schmidt and Bartlett 2002) for Z ; uncertainties in f_y are higher. Thus, only f_y , is defined herein as a random variable for the strength. The mean (μ) value, SD (σ) or COV and the assumed probability distributions for f_y are shown in Table 1.

The ductility of the structural sections are defined by the deformation parameters θ_y , θ_p and θ_{pc} of the modified IMK model; for W sections, these parameters can be determined by means of the following multi-variable empirical equations that were developed by Lignos and Krawinkler (2011, 2012, 2013):

$$\theta_y = (M_y/k_o)/L = (1.17 \cdot Z \cdot f_y/6 \cdot E \cdot I)/L \tag{1}$$

$$\theta_p = 0.0865 \cdot \left(\frac{h}{t_w}\right)^{-0.365} \cdot \left(\frac{b_f}{2 \cdot t_f}\right)^{-0.140} \cdot \left(\frac{L}{d}\right)^{0.340} \cdot \left(\frac{c_{unit}^1 \cdot d}{533}\right)^{-0.721} \cdot \left(\frac{c_{unit}^2 \cdot f_y}{355}\right)^{-0.721}$$

$$\sigma_{In} = 0.32 \tag{2}$$

$$\theta_{pc} = 5.63 \cdot \left(\frac{h}{t_w}\right)^{-0.565} \cdot \left(\frac{b_f}{2 \cdot t_f}\right)^{-0.800} \cdot \left(\frac{c_{unit}^1 \cdot d}{533}\right)^{-0.280} \cdot \left(\frac{c_{unit}^2 \cdot f_y}{355}\right)^{-0.430} \quad \sigma_{In} = 0.25 \tag{3}$$

Table 1 Probabilistic properties of strength and ductility variables

Type	Variable	Mean (μ)	SD (σ)	Function	Upper limit	Lower limit
Strength	f_y	375.76 Mpa ^a	26.68 (COV = 0.071) ^a	Normal distribution ^b	429.14 Mpa	322.4 Mpa
Ductility	θ_p	θ_p by Eq. (2)	$\sigma_{in} = 0.32$	Lognormal distribution ^c	θ_p by Eq. (2) + 2 σ_{in}	θ_p by Eq. (2) - 2 σ_{in}
Ductility	θ_{pc}	θ_{pc} by Eq. (3)	$\sigma_{in} = 0.25$	Lognormal distribution ^c	θ_{pc} by Eq. (3) + 2 σ_{in}	θ_{pc} by Eq. (3) - 2 σ_{in}

^aBased on the report by Lignos and Krawinkler (2012) for statistics of material yielding strength, obtained from flanges-webs tests for A572 grade steel

^bFor f_y the proposed function is based on the study by Lignos and Krawinkler (2012)

^cFor θ_p and θ_{pc} the proposed functions are based on Eqs. (2) and (3) presented in Lignos and Krawinkler (2011, 2012) respectively

In these equations, k_o is the initial elastic stiffness; I is the inertia moment; c_{unit}^1 and c_{unit}^2 are coefficients for unit conversion. h/t_w is the ratio between the web depth and the thickness; L/d is the ratio between the span and the depth of the beam; $b_f/(2 \cdot t_f)$ is the width/thickness ratio of the beam flange, and σ_{In} is the SD, assuming a lognormal fit of experimental data. Finally, the ultimate rotation capacity is estimated as $\theta_u = 1.5 \cdot (\theta_y + \theta_p)$, based on the recommendations of PEER/ATC 72-1 (2010). In this study, θ_y is considered a dependent variable of f_y , and θ_p and θ_{pc} are considered random variables with lognormal distributions. Mean (μ) values, SDs (σ_{In}) and function types used for θ_p and θ_{pc} are shown in Table 1. Uncertainties of θ_p (Eq. 2) and θ_{pc} (Eq. 3) also take into account the randomness of the dimensions of the W sections (Lignos and Krawinkler 2011, 2012, 2013), including uncertainties on I , h , d , t_w , b_f , t_f , and so on, as well as uncertainties on f_y .

Moreover, in order to avoid unrealistic samples in LHS simulations, both normal distributions of f_y and lognormal distributions of θ_p and θ_{pc} were truncated at both ends, the lower and upper limits being determined by the mean value ± 2 times the SD ($\mu \pm 2\sigma$). The purpose of this truncation is to avoid underestimates or overestimates of the capabilities of the elements with samples without physical meaning.

In summary, a simplified probabilistic approach is proposed for this research. The method uses the modified IMK model for beams and columns, and uncertainties are concentrated on the variables f_y , θ_p and θ_{pc} . Thus, it is assumed that these three variables have a major influence on the linear and non-linear structural response of buildings. Besides, the use of these variables is recommended in the new codes for probabilistic seismic performance assessment of steel buildings (PEER/ATC 72-1 2010; FEMA P-58-1 2012).

2.3 Correlation analysis

Another important issue concerning sampling is the correlation among variables. Two types of correlation have been considered in this research: intra- and inter-element. The intra-element correlation is given by the relation among the three parameters simulated for the same hinge; these correlations can be derived from Eqs. (2) and (3) (Lignos and Krawinkler 2012) and are defined in Table 2.

The inter-element correlation is attributed to the consistency in workmanship and the material’s quality among different element sections. Idota et al. (2009) and Kazantzi et al. (2014) proposed a value of 0.65 for the yield strength of beams and columns from the same production batch. Based on these studies, an inter-element correlation of 0.65 has been used herein for the same section type, and a null correlation is assumed for different sections.

2.4 Sampling

To better represent the physical randomness of the problem for each structural element (column or beam), a random sample of the three parameters (f_y , θ_p and θ_{pc}) is generated.

Table 2 Intra-element correlation for random variables of beams and columns

	f_y	θ_p	θ_{pc}
f_y	1	0	0
θ_p	0	1	0.69
θ_{pc}	0	0.69	1

Then, the properties of strength and ductility on the hinges of each element are estimated. It is assumed that hinges at both ends of elements are the same. Thus, for instance, the 3-storey model, with 27 elements (15 columns and 12 beams) has 81 random variables; the 7-storey building with 63 elements (35 columns and 28 beams) has 189 random variables; and the 13-storey model with 117 elements (65 columns and 52 beams) has 351 random variables. In order to assess the seismic behaviour of these three buildings, with a probabilistic approach, 200 NLSAs and 200 NLIDAs are performed for each structural model, resulting in 600 NLSAs and 600 NLIDAs. The same structural models are used for both structural analyses: static and dynamic. Figure 3b shows the modified IMK model for a null axial force, that is, pure bending used in the structural section (W16x89) of the SMF3 probabilistic models. The modified IMK model for pure bending is used to estimate the variable M_y (see Fig. 3a). Moreover, the critical buckling load and the nominal axial yield strength are used to estimate the axial load limits for compression and tension, respectively. In this way, the parameters for defining the interaction diagram relating the bending moment to the axial force, for each of the simulated random samples for the columns W16x89, are obtained.

3 Seismic actions

To perform probabilistic IDAs, a set of accelerograms representing the characteristics of the study area are needed. The way these acceleration time histories are obtained, is explained first, and the method is then applied to the Mexico City to obtain probabilistic response spectra and compatible acceleration time histories.

3.1 Method

In a first step, a set of random response spectra are generated by means of LHS simulations. The response spectra meet the following conditions: (1) the mean value is a target spectrum, (2) the SD in each period has a predefined value, and (3) the spectral ordinates are correlated in such a way that spectra are realistic. As an example, Fig. 4 shows a set of five simulated response spectra. The fundamental periods of the studied buildings are also depicted in this figure. Then, a spectral matching technique (Hancock et al. 2006), is used to match the response spectrum of a real accelerogram to each one of the simulated spectra. This way, a set of accelerograms that meet the above conditions can be obtained. Moreover, if the seed accelerogram is chosen properly, the spectrum-matched accelerograms are representative of the seismic actions expected in the area.

3.2 Probabilistic response spectra

In this study, the design spectrum for area III_b of the NTC-DF (2004) in Mexico City has been taken as the target spectrum. Moreover, the SD has been set to 5% for periods from 0 to 2 s, corresponding to the range in which the periods of the buildings are situated, and 10% for periods greater than 2 s, thus controlling uncertainties in seismic actions. The 5 and 10% intervals for SDs were chosen on the basis of FEMA P-1051 (2016) recommendations, about the use of spectral matching of ground motions; These recommendations establish that the matched spectra should not be outside the range of + or – 10% of the target spectrum.

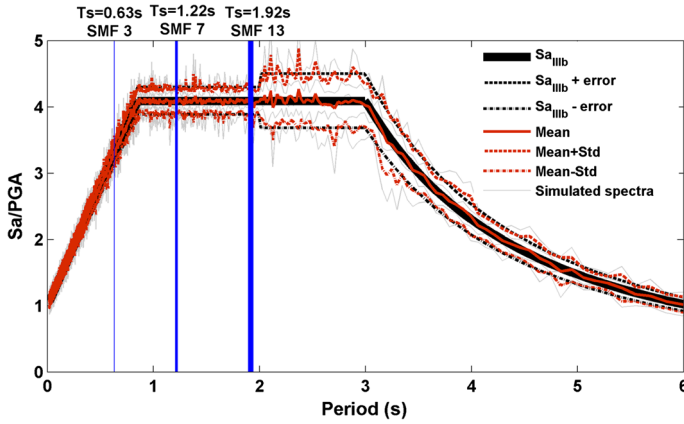


Fig. 4 Five simulated response spectra. Mean and SD conditions are also shown. The five simulated spectra are used to match accelerogram acc1 (see Table 3)

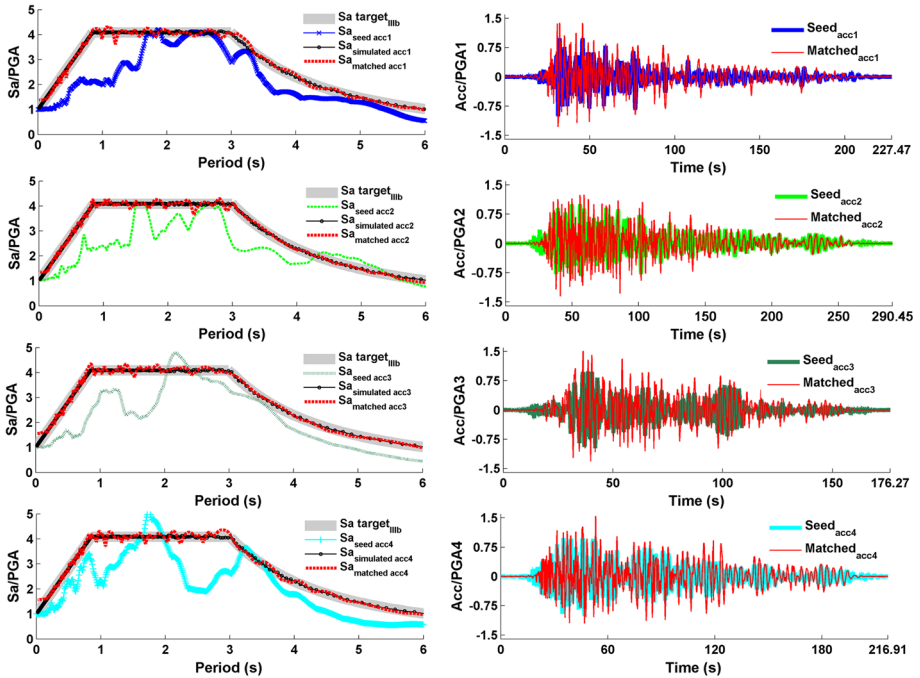


Fig. 5 Target spectrum and response spectra of the seed and matched accelerograms (right). Seed and matched accelerograms (left)

3.3 Probabilistic acceleration time histories

A preliminary set of time histories was selected using the method proposed by Vargas et al. (2013). A large database of 2554 accelerograms (three components) recorded in the Mexico City area was used. Thus, four accelerograms with a relatively high compatibility

Table 3 Characteristics of seed accelerograms selected by the Vargas et al. (2013) method

Acc.	Station	Date	Duration (s) ^a	Epicentre		Magnitude (Mw)	Component	PGA (cm/s ²)	Epicentral distance (km)	Azimut Star-Epi
				Latitude	Longitude					
acc1	TH35	20/03/12	227.47	16.25N	98.52W	16	S00E	49.6	340.58	171.34
acc2	AE02	30/09/99	290.45	15.95N	97.03W	16	N90W	21.3	442.48	150.64
acc3	PCSE	11/01/97	176.27	17.91N	103.04W	16	S65W	14.6	442.84	248.35
acc4	DM12	14/09/95	216.91	16.31N	98.88W	22	N00E	19.3	347.79	176.20

^aDuration refers to the total length of the accelerogram, including added time before and after event recording

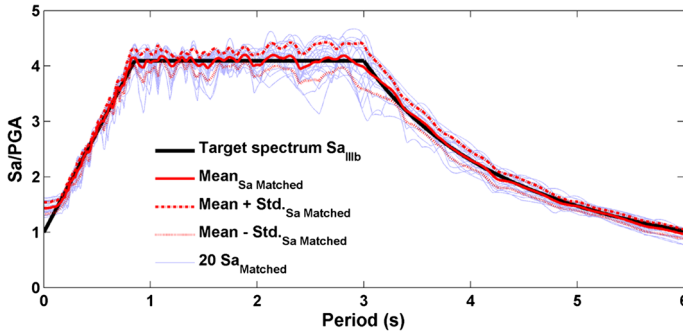


Fig. 6 Response spectra of the 20 accelerograms; mean and SDs are also depicted

with the target spectrum were selected. Then a spectral matching technique was used to improve the fit between response spectra of seed accelerograms and the target spectrum. Figure 5 shows the seed accelerograms that have been selected, the matched ones and the corresponding response spectra. This large database of Mexican accelerograms was previously analysed by Diaz et al. (2015). Table 3 shows the characteristics of the four selected accelerograms and corresponding earthquakes. The PGA values are low, with a maximum PGA value of 49.6 cm/s^2 . This is due to the large epicentral distances of the earthquakes affecting Mexico City.

No near-fault seismic actions are expected, as the seismic hazard of the city is dominated by the combined effects of distant, large earthquakes and soil amplification, leading to increased PGA values and long-duration acceleration records. These were the main causes of the destructive 1985 Michoacán earthquake. However, as shown below, the newly developed methods are valid for low and high PGA values, as both the capacity spectrum method and the NLIDA, allow any PGA value to be set for seismic actions affecting the buildings.

Spectral matching warranties the similarity between the shapes of the response spectra of the matched accelerograms and the code-provided design spectra, but both signals and spectra can be scaled to any PGA value, thus representing any level of seismic intensity well. In fact, in this study, PGA values have been set in the range between 0.05 and 0.7 g. Thus, for each seed accelerogram, the spectral matching technique was used to obtain 5 new accelerograms meeting the probabilistic requirements described above. As a result, a set of 20 accelerograms were obtained. This number of accelerograms was considered adequate, as the Mexican seismic code (NTC-DF 2004) suggests that at least four accelerograms should be used. Twenty acceleration time histories was also considered a suitable number to deal with uncertainties in seismic actions, as they represent the pre-assumed probabilistic distributions well (see Figs. 4, 8). The whole set of response spectra corresponding to the 20 compatible accelerograms is shown in Fig. 6.

4 Probabilistic IDA

In this section, the influence that the randomness of the mechanical properties and the uncertainty of the seismic actions have on the uncertainties of the structural response is analysed and discussed. The analysis is shown for the low-rise buildings; similar conclusions also hold for mid- and high-rise buildings.

4.1 Adequacy of the sampling

4.1.1 Mechanical properties

As pointed out above, 200 realizations of random structural parameters are used. This number has been determined in the following way. A number of random samples are generated according the truncated predefined probability density function (pdf). After every 20 new samples, the mean value and the SD of the overall samples are obtained. For more than 200 samples no significant variations are obtained in their mean value and SD so that 200 has been considered an adequate number of samples representing the predefined truncated pdf. In fact, the LHS technique avoids duplicating case combinations, so that fewer samples adequately represent the target pdf (Iman 1999). Moreover, other authors have also used 200 probabilistic models to assess the seismic performance of buildings (Fragiadakis and Vamvatsikos 2008; Kazantzi et al. 2008). Figure 7 shows the target normal and normal truncated pdfs together with the histogram of the 200 samples for the f_y random variable. A good agreement between histogram and the target pdfs can be seen. Similar plots can be depicted for the other random variables.

4.1.2 Seismic actions

For each probabilistic IDA, only 20 accelerograms are used. In order to see that 20 time histories adequately represent the foreseen uncertainties, so that actually 20 samples are sufficient for the probabilistic approach, the following analysis is performed. In fact, uncertainties in each acceleration time history affects all the periods of the response spectrum, that is, the response is affected by the uncertainty at all the periods. For each period, these uncertainties have been predefined by means of a normal pdf function that has the target spectrum as a mean value and a predefined SD, which is 5%, in the period range 0–2 s, and 10%, in the period range 2–6 s.

To illustrate how these distributions are well fulfilled by the 20 accelerograms, Fig. 8a, b have been obtained as follows. For each one of the twenty response spectra matched by the seed accelerograms, the simulated random values, at each period, have been

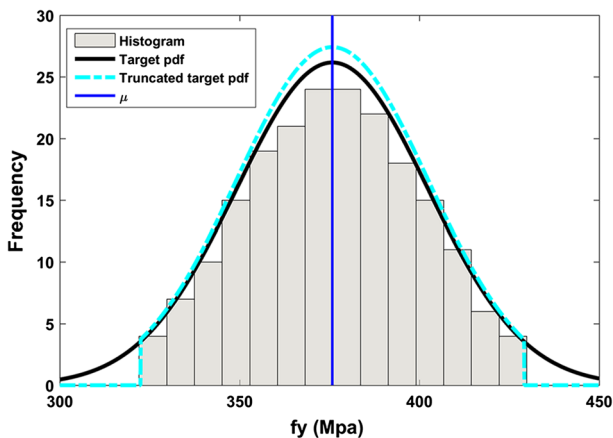


Fig. 7 Histogram of the 200 samples of the f_y and corresponding scaled pdf target functions

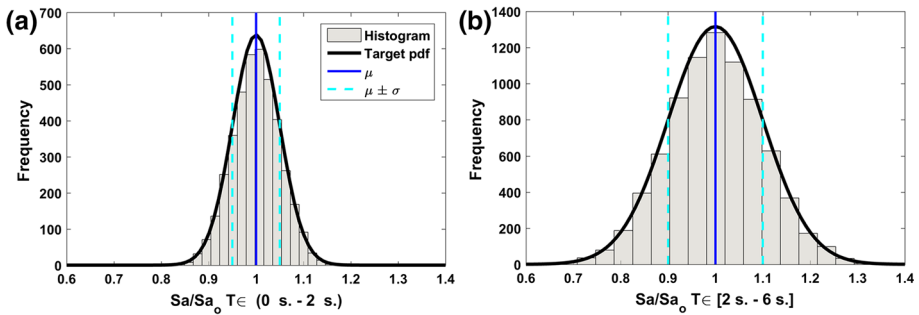


Fig. 8 Histogram of the samples used to define the seismic actions in a probabilistic way. Scaled target pdf functions are also shown. **a** In the period range (0–2) s and **b** in the period range [2–6] s (see also explanation in the text)

normalized by the value of the mean spectrum, in such a way that the normalized samples have a unit mean and the predefined SD. Figure 8a corresponds to the samples in the period range (0–2) s and Fig. 8b corresponds to the period range [2–6] s. It can be seen how the twenty selected accelerograms adequately represent the predefined uncertainties with a unit mean (value of the mean target spectrum), and 0.05 and 0.1 SDs, respectively for the short and long period ranges. This way it can be seen how the 20 accelerograms adequately represent the predefined mean values and foreseen uncertainties. Moreover, several probabilistic approaches in the literature (Kazantzi et al. 2008; Asgarian et al. 2010; Celarec and Dolšek 2013; Vargas et al. 2013) use suites of 15–20 accelerograms. Besides, Vamvatsikos (2014) proposes to limit the computational cost of probabilistic IDA evaluations reducing the size of the ground motion records. Thus, if an incremental sampling technique (Sallaberry et al. 2008; Vamvatsikos 2014) or some justified criterion is used, the time histories can be reused. In this research it has been assumed that each accelerogram can be reused, mainly because of the two following reasons: (1) as shown above, (see Fig. 8a, b) the probabilistic spectral matching technique warrants the pre-assumed probability distributions in the uncertainties of the 20 seismic actions (see also Fig. 6), and (2) on the basis of the principle that, all the records in the suite have the same probability of occurrence.

4.2 Uncertainty in the response

A total of 200 SMF3 structural models with the variables obtained from LHS Monte Carlo simulations and the set of 20 compatible seismic actions are used. The analyses are performed in such a way that the influence of the mechanical properties (f_y , θ_p , θ_{pc}) and the impact of the seismic actions can be analysed separately.

NLIDA has been performed for different PGAs covering the range between 0.05 and 0.7 g, with PGA increments of 0.05 g. The following cases are analysed. First, the building is considered as deterministic while the seismic action is considered as probabilistic by using the 20 matched accelerograms; then the seismic action is considered as deterministic by using the acc1 (see Table 3 and Fig. 5), matched to the selected target spectrum as explained above. Thus, the following five cases are considered: (1) the building is considered deterministic and seismic actions probabilistic; (2) seismic action deterministic and building probabilistic by considering uncertainties in the three mechanical properties (f_y , θ_p and θ_{pc}). In the following cases, the seismic action is considered in a deterministic way

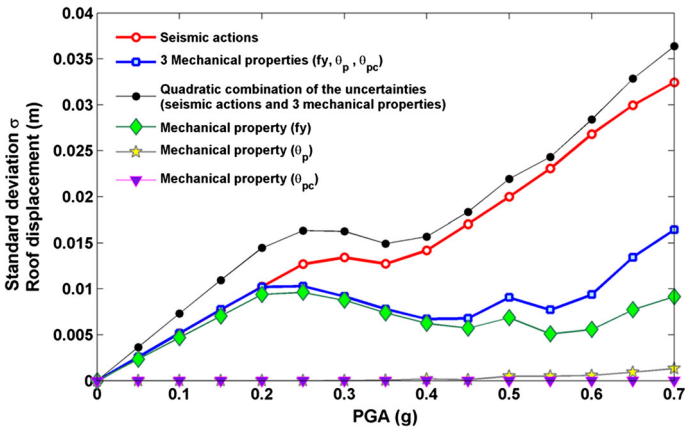


Fig. 9 Uncertainties in the roof displacement for the SMF3 building (see the discussion in the text)

and only uncertainties for one of the mechanical properties are considered according to the following cases: (3) f_y , (4) θ_p and (5) θ_{pc} . In all these five cases and for each PGA, the SD (σ) in the structural response is computed; the roof displacement δ is considered a control variable of the response. Figure 9 shows the results obtained. In addition to the uncertainties in the roof displacement for the five cases described above, the overall uncertainty is shown in this figure. This total uncertainty is obtained using the well-known quadratic composition (Vargas et al. 2013). As expected, uncertainties due to uncertainties in θ_p and θ_{pc} are small compared to those induced by uncertainties in f_y ; but uncertainties due to θ_p and θ_{pc} have a significant influence when they are combined with those due to f_y . The influence of uncertainties in seismic actions is clearly dominant. Probably, with the exception of θ_{pc} , uncertainties in the response tend to increase with increasing seismic actions. Similar results, concerning the influence of uncertainties in seismic actions and the increase of uncertainties with increasing seismic actions, were reported for reinforced concrete buildings in Vargas et al. (2013). The increase of uncertainties with increasing actions may be attributed to the fact that, for increasing PGA, the damage also increases, and the structural system becomes unstable, in the sense that small input variations produce considerable differences in the output.

5 Parametric model

In this section, the parametric model for capacity curves (Pujades et al. 2015) is applied. Deterministic and probabilistic cases are analysed. Mean values of strength-ductility of the sections are used for the deterministic approach and, as pointed out above, 600 models generated by LHS Monte Carlo techniques are used for the probabilistic approach.

5.1 Capacity curves

Capacity curves have been obtained by means of adaptive pushover analysis (PA) (Satyarno 2000) as implemented in the Ruaumoko software (Carr 2002). This method was shown to be independent from the initial loading pattern, as it adapts this pattern at each step of the PA, according to the deformation of the structure. The ultimate capacity is

established when one of the following criteria is fulfilled. (1) ω^2 is less than $10^{-6} \omega^2$ at the first step, being ω the tangent fundamental natural frequency in the Modified Rayleigh Method; (2) the Newton–Raphson iteration is not achieved within a specified maximum number of cycles; (3) the stiffness matrix becomes singular and (4) a specified maximum structure displacement is reached. In the NLSAs of the studied buildings, a large number of cycles for the Newton–Raphson method has been considered. Moreover, a large maximum limit for the structure displacement has been considered. Thus, it is expected that failure criteria be related to criteria (1) or (3) it is worth noting that the failure criterion is usually fulfilled when plasticization occurs in all the pillars of a story.

Figure 10 shows the obtained capacity curves. For comparison purposes the 5th, 50th and 95th percentiles are used. The following steps have been carried out to obtain a specific nth percentile: (1) capacity curves are interpolated/extrapolated in such a way that they are defined at the same points in the same interval; a fixed small displacement increment, $\Delta\delta$, is used to this end and the interval between 0 and the maximum ultimate displacement is used; (2) for each spectral displacement, ordinates are sorted from lowest to highest values, (3) the nth percentile is computed at each spectral displacement, (4) the ultimate displacement of the nth percentile is set to the nth percentile of the ultimate displacements. The 5th, 50th and 95th percentiles, computed this way, are shown in Fig. 10. Deterministic capacity curve and the 200 individual probabilistic capacity curves are also shown in this figure.

The 50th percentile curves (median) match the deterministic curves well, although the matching is better for SMF3 and SMF7 models. Differences between deterministic and median capacity curves are in the non-linear zone and they can be attributed mainly to non-

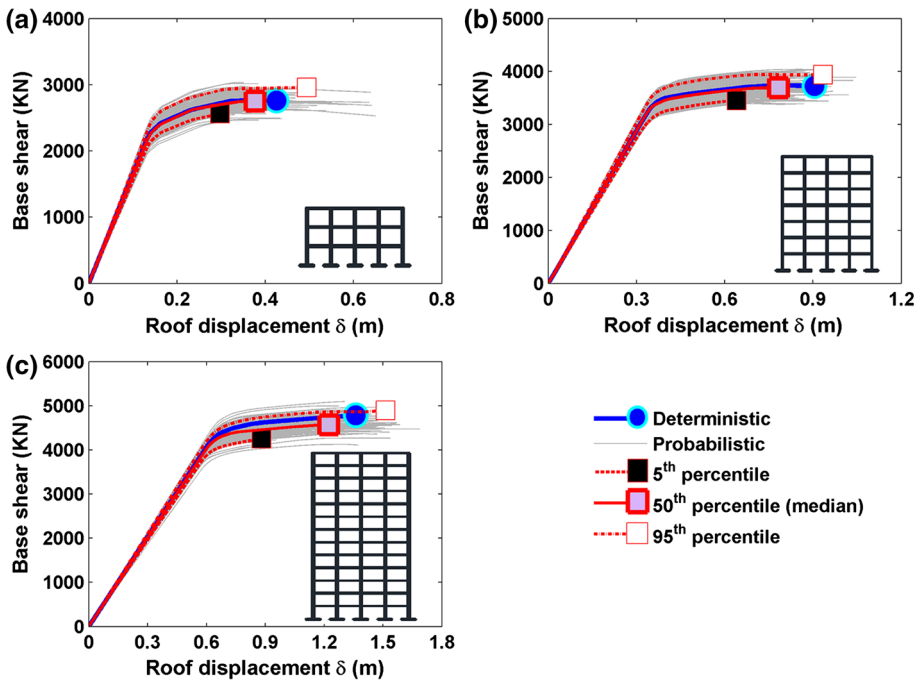


Fig. 10 Deterministic, probabilistic and percentiles of the capacity curves. **a** SMF 3, **b** SMF 7 and **c** SMF 13

linearity of the structural response. The fact that individual points of the median curve correspond to different capacity curves can also contribute to these differences.

5.2 Capacity model

The parametric model for capacity curves/spectra is well-described in Pujades et al. (2015). To test this model, capacity spectra have been preferred rather than capacity curves. Table 4 displays the weights, w_i and the normalized amplitudes Φ_{i1} , at level i , for the first natural mode. Table 5 shows the total weight, W , of the building and the period, T_1 , modal participation factor, PF_1 , and modal mass coefficient, α_1 , for the first natural mode. Note that Φ_{roof1} , PF_1 and, α_1 , are used to transform capacity curves into capacity spectra (ATC 40 1996).

The five parameters that fully define the capacity spectrum are the initial slope (m), the mean value (μ) and the SD (σ) of the lognormal function and the ultimate capacity point (S_{d_u} , S_{a_u}). m is related to the initial stiffness and to the period of the fundamental mode of vibration; the cumulative lognormal function, defined by μ and σ , fits the normalized first derivative of the non-linear part of the capacity spectrum.

Figure 11 displays the model as applied to the median capacity spectra of the three buildings. Capacity spectra, together with their linear and non-linear parts, are shown (upper part); first derivatives are shown in the lower part of this figure. Figure 12 shows the individual and the deterministic capacity spectra; the obtained fits are also displayed.

The five parameters of the deterministic case and 5th, 50th and 95th percentiles are given in Table 6. The mean values of the error vectors (% Mean error) defined by the difference, in percentage, between capacity spectra and the corresponding fit, are also provided in this table. Mean errors are very small (always below the 3%). Note the likeness between the parameters of the deterministic and 50th percentile capacity spectra.

6 Damage

An important issue related to seismic design of new buildings and, specially, related to seismic risk assessment of existing structures and facilities is the expected damage. A widely used damage index is the Park and Ang damage index (Park 1984; Park and Ang 1985; Park et al. 1985, 1987). We refer to this damage index as DI_{PA} . According to the Park and Ang studies, structures are damaged because of the combined effects of displacements in the nonlinear range due to their response to large stresses and of cyclic drifts in response to cyclic strains. Therefore, damage assessment must take into account also repeated cyclic loads/unloads, in addition to maximum structural response. Displacements in the nonlinear range are related to stiffness degradation and cyclic loadings are related to energy losses. This idea is based on the damage index proposed by Pujades et al. (2015), which is also based on two functions related to stiffness degradation and to energy loss; but now, these functions are computed, in a straightforward way, from capacity curves or capacity spectra. We refer to this new capacity-based-damage index as DI_{CC} . Many computer programs for structural analysis, as Ruaumoko 2D (Carr 2002) in our case, implement the Park and Ang damage index DI_{PA} , so that it can be obtained by means of Non-Linear-Incremental-Dynamic-Analysis (NLIDA). The following equation defines this damage index:

Table 4 Weights, w_i , and normalized amplitude of the first natural mode, ϕ_i

	Storey	1	2	3	4	5	6	7	8	9	10	11	12	13
SMF3	w_i (KN)	885.9	881.4	605.6										
	ϕ_i	0.4	0.775	1										
SMF7	w_i (KN)	902.6	890.6	890.6	889.6	881.4	881.4	605.6						
	ϕ_i	0.133	0.313	0.489	0.647	0.803	0.929	1						
SMF13	w_i (KN)	924.5	909.7	909.7	909.7	909.7	903.2	890.6	890.6	890.6	889.6	881.4	881.4	605.6
	ϕ_i	0.057	0.135	0.219	0.303	0.384	0.463	0.563	0.664	0.755	0.832	0.906	0.965	1

Table 5 Total weight, W , and period, T_1 , modal participation factor, PF_1 , and modal mass coefficient, α_1 , for the first natural mode

Building	W (kN)	T_1 (s)	PF_1	α_1
SMF3	2372.9	0.63	1.286	0.891
SMF7	5941.8	1.22	1.350	0.805
SMF13	11,396.3	1.92	1.397	0.754

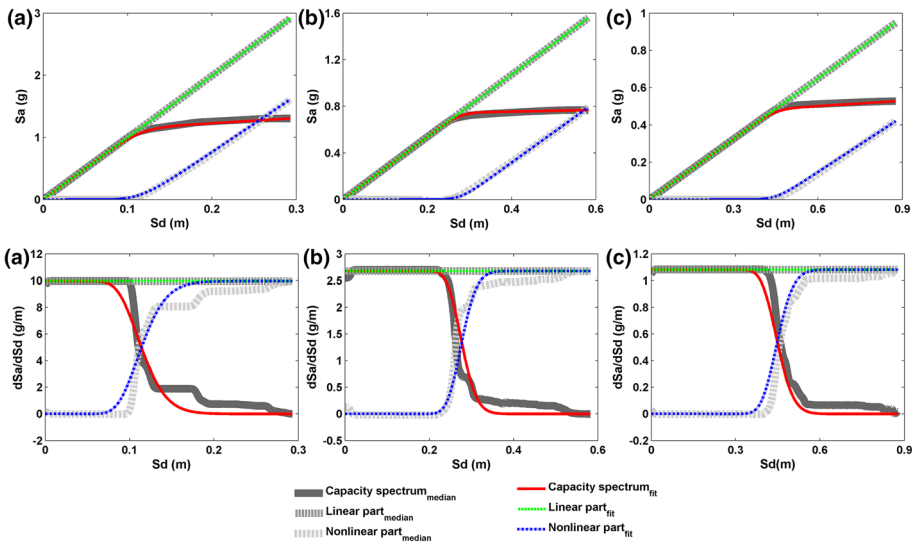


Fig. 11 Capacity spectrum, linear part and non-linear part (up) and corresponding first derivatives (down). Fits for the 50th percentile of the probabilistic capacity spectra are also shown. **a** SMF 3, **b** SMF 7 and **c** SMF 13

$$DI_{PA} = \frac{\delta}{\delta_u} + \frac{\beta}{Q_y \delta_u} \int_0^{\delta} dE \tag{4}$$

where δ/δ_u is the ductility, defined as the ratio between the maximum displacement of the structural element subjected to a specific earthquake, δ , and the ultimate displacement under monotonic loading, δ_u . Q_y is the strength at the yielding point. If the strength, Q_u , corresponding to the ultimate displacement, δ_u , is lower than Q_y , then Q_y is substituted by Q_u . $\int_0^{\delta} dE$ represents the hysteretic energy absorbed by the element during the earthquake and β is an empirical non-negative coefficient. Park et al. (1987), Ghosh et al. (2011) and Kamaris et al. (2013) have shown that $\beta = 0.025$ is a good approximation for steel buildings. Ruaumoko 2D program has been used to perform NLIDA and to compute DI_{PA} . Further details on how the DI_{PA} is implemented can be found in the Ruaumoko 2D technical manual (Carr 2002). In this section, DI_{PA} and DI_{CC} are computed for the analysed steel buildings. Notice that, according to Pujades et al. (2015) DI_{PA} is needed to calibrate the relative contribution to damage of the stiffness degradation and of the energy loss.

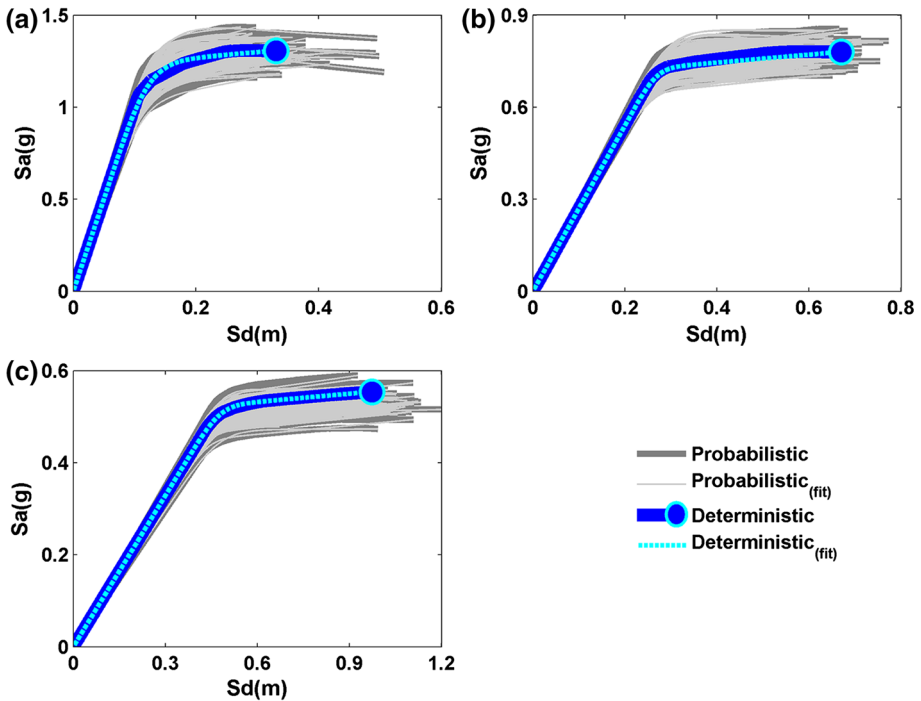


Fig. 12 Probabilistic capacity spectra and fits. The deterministic case is also shown. **a** SMF 3, **b** SMF 7 and **c** SMF 13

6.1 Park and Ang damage index (DI_{PA})

Ruamoko 2D is used to compute DI_{PA} through NLIDA. Notably, the failure or ultimate point in the NLIDA is defined by the first roof displacement that exceeds the ultimate displacement of the corresponding capacity curve. Usually at this point, DI_{PA} is about 1, which confirms a failure condition. To obtain probabilistic DI_{PA} with NLIDA, the suite of 20 accelerograms, whose response spectra have controlled mean and SD, are used as follows. Accelerograms in the suite are organized and they are numbered between 1 and 20. Then, in each of the 200 IDA, an integer random number, uniformly distributed between 1 and 20, is generated. The accelerogram having assigned this random number is used for the corresponding IDA analysis. The adequacy of this procedure for the purpose of this study has been also discussed above (see Sect. 4.1.2 and Fig. 8). To obtain DI_{PA} in a deterministic way, the mean of the four matched accelerograms, shown in Fig. 5, is used. This way a deterministic and 200 probabilistic functions, linking the roof displacement, δ , and the Park and Ang damage index, DI_{PA} are obtained. Again, the 5th, 50th and 95th percentiles are used for discussion. The procedure to obtain these percentile curves has been briefly explained above. Figure 13 shows the results obtained for the SMF 3, SMF7 and SMF 13 building models.

For the deterministic NLIDAs, the mean of the four matched accelerograms shown in Fig. 5 is used. The δ - DI_{PA} functions for the studied buildings are shown in Fig. 13. Observe how deterministic DI_{PA} s are lower than the probabilistic 50th percentile. Because of nonlinearity of the structural response, the use of mean, median or characteristic values

Table 6 Parameters of the capacity model for the deterministic capacity curve and for the 5th, 50th and 95th percentiles of the probabilistic capacity spectra

	SMF3					SMF7					SMF13							
	m (g/m)	Sdu (m)	Sau (g)	μ	σ	% Mean error	m (g/m)	Sdu (m)	Sau (g)	μ	σ	% Mean error	m (g/m)	Sdu (m)	Sau (g)	μ	σ	% Mean error
Deterministic	10.05	0.33	1.31	0.37	0.25	0.17	2.70	0.67	0.78	0.40	0.10	0.77	1.10	0.97	0.55	0.49	0.10	0.06
5th percentile	9.44	0.23	1.21	0.48	0.10	0.25	2.55	0.48	0.72	0.58	0.15	0.65	1.04	0.63	0.49	0.70	0.05	0.01
Median	9.96	0.29	1.30	0.39	0.20	1.18	2.68	0.58	0.77	0.48	0.10	0.55	1.08	0.88	0.53	0.51	0.10	0.93
95th percentile	10.67	0.38	1.40	0.30	0.15	2.74	2.84	0.69	0.83	0.39	0.10	0.84	1.12	1.09	0.57	0.46	0.15	1.26

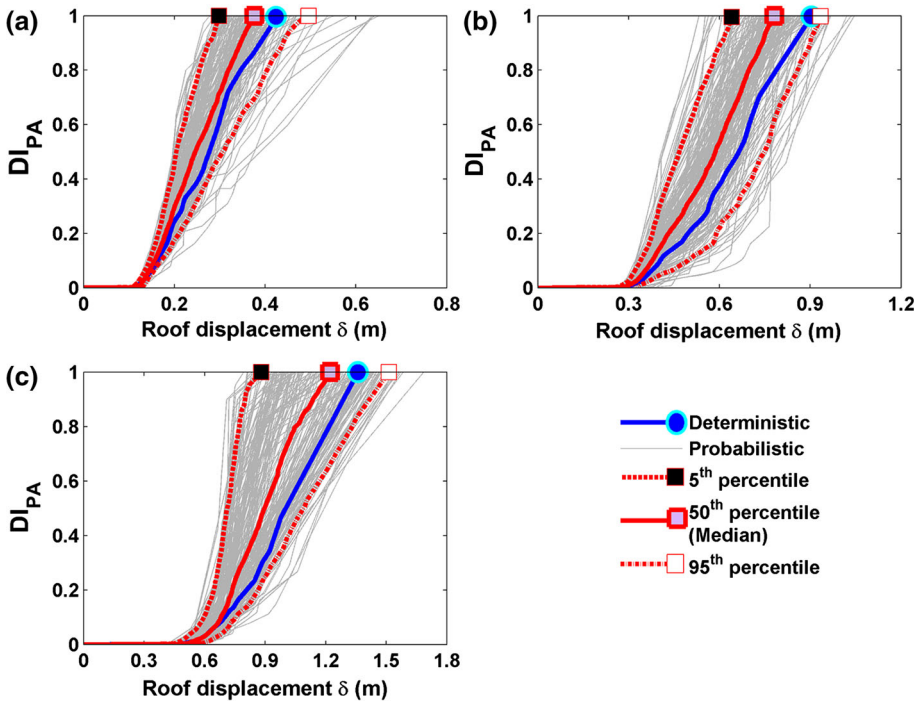


Fig. 13 δ - DI_{PA} functions obtained with NLIDAs for: a SMF 3, b SMF 7 and c SMF 13

does not guarantee to get mean, median or characteristic responses. This fact highlights the importance of probabilistic approaches in front of the more frequently used deterministic approaches. Note that, in the case of Fig. 13, the use of mean values, both of the seismic actions and strength parameters, leads to un-conservative results, which emphasizes, even more, the importance of probabilistic approaches.

6.2 Capacity-based damage index (DI_{CC})

DI_{CC} is based on the combination of a stiffness degradation function, $K(\delta)$, and an energy dissipation function, $E(\delta)$. The computation of these functions is well-described in Pujades et al. (2015). However, for clarity, a basic explanation of how these functions are defined is also given herein. $E(\delta)$ is defined by the cumulative integral of the non-linear part of the capacity curve; the obtained function is then normalized, in abscissae and in ordinates, to obtain the normalized $E_N(\delta_N)$, ranging between 0 and 1 and also taking values between 0 and 1. $K(\delta)$ is defined by the ratio between the ordinates and abscissae of the non-linear part of the capacity curve; again, normalizing in abscissae and in ordinates, the $K_N(\delta_N)$ function is obtained. DI_{CC} is defined by the following equation:

$$DI_{CC}(\delta_N) = \alpha K_N(\delta_N) + (1 - \alpha)E_N(\delta_N) \cong DI_{PA} \tag{5}$$

where $E_N(\delta_N)$ and $K_N(\delta_N)$ are the normalized energy and stiffness functions defined above, and α is a parameter that defines the relative contributions to the damage index of the stiffness degradation and that of the energy loss. The specific value of this parameter α , for a given seismic action, is calibrated by means of a least squares procedure applied to

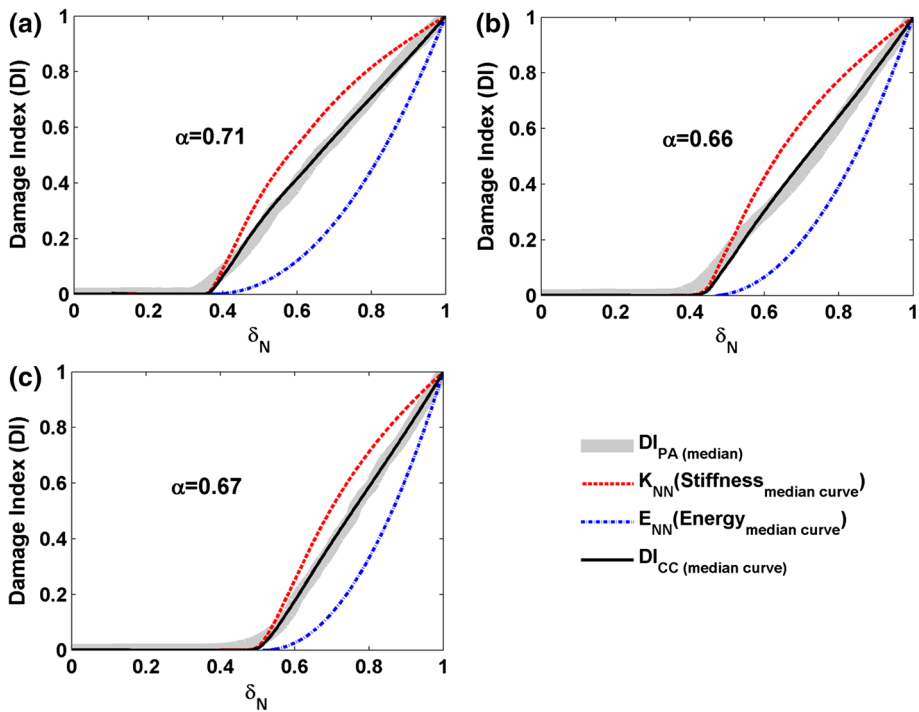


Fig. 14 Energy and stiffness degradation functions and calibration of the $DI_{CC}(\delta_N)$ for the median capacity curve. **a** SMF 3, **b** SMF 7 and **c** SMF 13

Eq. (5). This way this new damage index, DI_{CC} , is equivalent to DI_{PA} . Specific examples of $E_N(\delta_N)$, $K_N(\delta_N)$, $DI_{CC}(\delta_N)$ and $DI_{PA}(\delta_N)$ are shown below, in the following section (Fig. 14), where the results of the calibration of Eq. (5) are discussed.

6.3 Results and discussion

For the three analysed buildings, the calibration is illustrated for the median capacity curves using median DI_{PA} s. Thus, the $K_N(\delta_N)$, $E_N(\delta_N)$ and $DI_{PA}(\delta_N)$ functions are used to calibrate the parameter α , by means of a least squares fit of Eq. (5). α values are 0.71, 0.66 and 0.67 for SMF3, SMF7 and SMF13 buildings respectively. Figure 14 shows these three cases. Undoing the normalization procedure these functions can be represented as functions of the roof displacements δ . Figure 15 shows $DI_{PA}(\delta)$ and $DI_{CC}(\delta)$ for the deterministic case and for the 5th, 50th and 95th percentiles capacity curves. The obtained values of α are in the range between 0.66 and 0.71, which is also similar to the range reported by Pujades et al. (2015) for reinforced concrete buildings. Thus, $DI_{PA}(\text{median})$ is well-represented by the new damage index $DI_{CC}(\text{median})$ obtained directly from the capacity curves. As explained above, the value of α is directly related to the relative contribution to damage of the secant stiffness degradation, while $(1-\alpha)$ corresponds to the relative contribution of the energy loss. In the case of the median DI_{CC} of Fig. 15, contributions to damage of the stiffness degradation are in the range 66–71%, while the contribution of the energy loss is in the range 29–34%.

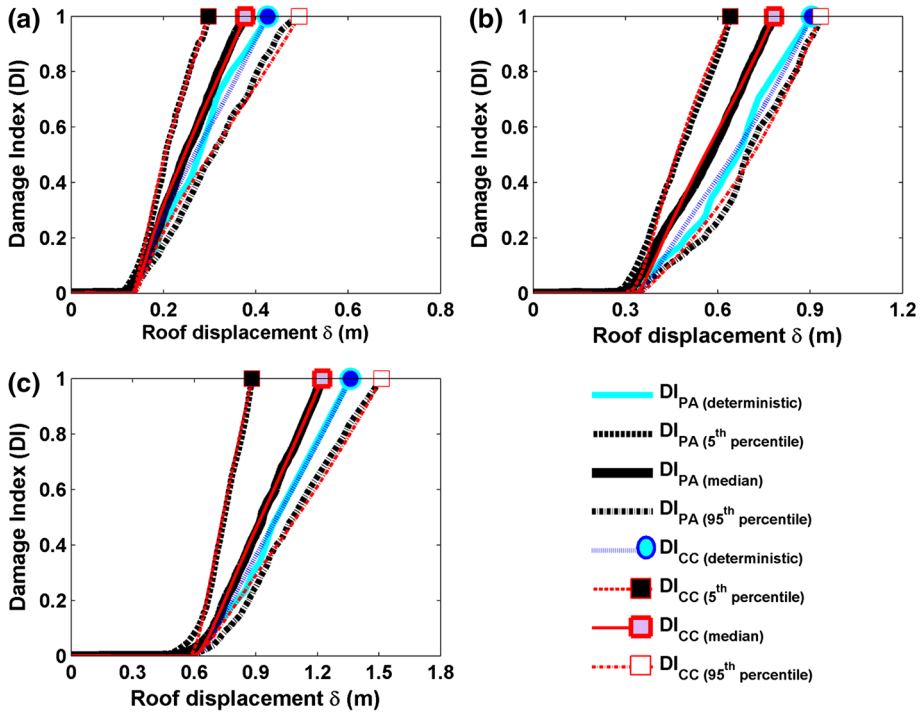


Fig. 15 DI_{CC} and DI_{PA} for the deterministic case and for the 5th, 50th and 95th percentiles. **a** SMF 3, **b** SMF 7 and **c** SMF 13

7 Fragility

Fragility curves and damage probability matrices are widely used in earthquake engineering (FEMA 2016; Milutinovic and Trendafiloski 2003; Lagomarsino and Giovinazzi 2006). Porter (2017) is a nice tutorial for beginners (see also Porter et al. 2007). Details of the construction of fragility curves, in the framework of our research, are explained well in Lantada et al. (2009, 2010), Vargas et al. (2013) and Pujades et al. (2012). In this section, the basics of fragility curves, damage probability matrices and mean damage state are described first; then, the specific damage states thresholds used are introduced; finally, the obtained results are given and discussed.

7.1 Basics

In the earthquake engineering context, for a given damage condition or damage state, i , and for a level of seismic intensity measure, IM , the fragility curve, $F_i(IM)$, is defined as the probability that this damage state be exceeded, given the seismic intensity SI . Thus, fragility curves are usually given as functions of a variable (SI) linked to the severity of the seismic action such as, for instance, spectral displacement, PGA or macroseismic intensity, among others. The spectral displacement, S_d , is used herein. Fragility curves are commonly modelled by means of cumulative lognormal functions defined by two parameters, μ_i and β_i . μ_i is the median of the lognormal function and is known as i -damage state

threshold; β_i is related to the dispersion of the lognormal cumulative function. In this research four non-null damage states are considered: (1) *Slight*, (2) *Moderate*, (3) *Severe* and (4) *Complete*.

The main hypothesis underlying the construction of fragility curves herein are the following: (a) damage states thresholds, that is μ_i , are determined from capacity curve or from other criterion based, for instance, on observational data or expert opinion, and (b) the assumption that expected damage follows a binomial distribution (Grünthal 1998; Lagomarsino and Giovinazzi 2006) allows determining β_i . Be aware that the probability of exceedance in the damage state thresholds, μ_i , is 0.5; To decide the spectral displacements damage thresholds, two procedures are used here. The first one (Lagomarsino and Giovinazzi 2006) was proposed in the framework of the European Risk-UE project (see Milutinovic and Trendafiloski 2003) and is based on the bilinear form of the capacity curve, which is defined by the yielding point (S_{dy} , S_{ay}) and the ultimate capacity point (S_{du} , S_{au}). Thus, the Risk-UE based damage state thresholds are defined as follows:

$$\mu_1 = 0.7S_{dy}; \quad \mu_2 = S_{dy}; \quad \mu_3 = S_{dy} + 0.25(S_{du} - S_{dy}); \quad \mu_4 = S_{du} \quad (6)$$

The second one (Pujades et al. (2015) is based on DI_{PA} , or in its equivalent DI_{CC} , damage index. Spectral displacements corresponding to damage index (DI_{PA} or DI_{CC}) values of 0.05, 0.2, 0.4, and 0.65, are allotted to the thresholds of the damage states *Slight*, *Moderate*, *Severe*, and *Complete*, respectively. Recall that these values are based on damage observations (Park et al. 1985, 1987; Cosenza and Manfredi 2000). This way fragility curves for the four damage states are set up.

Fragility curves easily allow us to obtain damage probability matrices (DPM), that is, the probability of the damage states $P_i(S_d)$. Then the mean damage state can be obtained, $D(S_d)$, also as a function of the same variable used to define fragility curves; often, the normalized mean damage state, $MDS(S_d)$ is used; how DMP, $D(S_d)$ and $MDS(S_d)$ are obtained from fragility curves is shown below. Once the fragility curves, $F_k(S_d)$, $k = 1, \dots, 4$, are known, for each spectral displacement, S_d , $P_j(S_d)$, define the probability of the damage state j as a function of the spectral displacement, S_d . Equation (7) shows how these probabilities are obtained from fragility curves:

$$P_0(S_d) = 1 - F_1(S_d); \quad P_j(S_d) = F_j(S_d) - F_{j+1}(S_d) \quad j = 1 \dots 3 \quad P_4(S_d) = F_4(S_d) \quad (7)$$

P_0 corresponds to the probability of the null damage state, while indices 1–4 correspond to the four non-null damage states. Then the following equation defines the mean damage state $D(S_d)$ and the normalized mean damage state, $MDS(S_d)$:

$$D(S_d) = \sum_{j=0}^4 jP_j(S_d) = 4MDS(S_d) \quad (8)$$

As discussed in Pujades et al. (2015), MDS should not be compared directly with DI_{PA} because MDS has a statistical meaning and is based on the thresholds of the defined damage states, while DI_{PA} must be interpreted as a physical pointer, linked to the progressive degradation of the bearing capacity of the building.

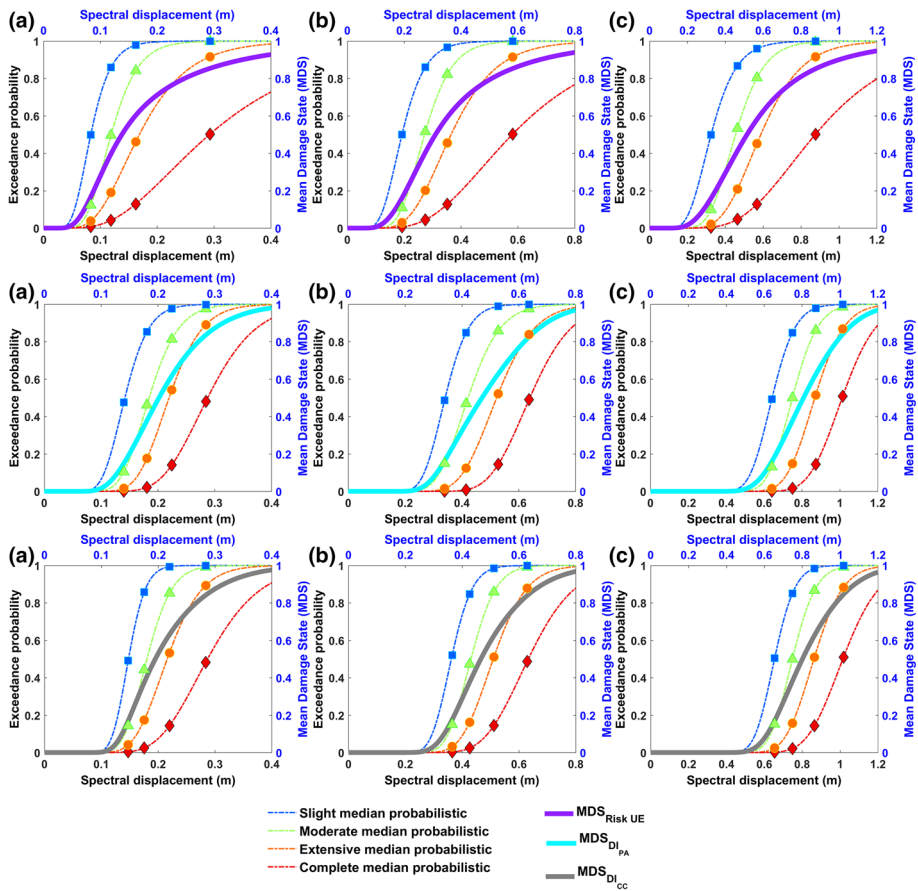


Fig. 16 Fragility curves and MDS functions obtained for median capacity spectra. Row 1 shows the case based on the Risk-UE project, row 2 shows the case based on DI_{PA} , and row 3 shows the case based on DI_{CC} . **a** SMF 3, **b** SMF 7, **c** SMF 13, **a** SMF 3, **b** SMF 7, **c** SMF 13, **a** SMF 3, **b** SMF 7, **c** SMF 13

7.2 Results

Figure 16 shows the fragility curves, F_j , and the normalized mean damage state, MDS, as functions of spectral displacement. In this figure, the first row shows the case based on the Risk-UE project for the median capacity spectra shown in Fig. 11; the second row corresponds to damage state thresholds based on the median DI_{PA} ; row 3 shows the case of the median DI_{CC} . Median DI_{PA} and DI_{CC} damage indices are shown in Fig. 15. Table 7 shows the parameters of these fragility curves (S_{d_i} , μ_i and β_i) for the deterministic and probabilistic 5th, 50th and 95th percentiles. The upper part of this table, corresponds to Risk-UE based fragility curves, in the middle the parameters corresponding to fragility curves based on DI_{PA} are given and the lower part shows the parameters of the fragility curves based on DI_{CC} . In fact, both indices are almost equivalent as DI_{PA} , has been used to fit DI_{CC} . Thus, the corresponding fragility and MDS functions are also similar. The μ_i and β_i values in the shadowy area correspond to the fragility curves of Fig. 16. Moreover, Fig. 17 compares the MDS functions, as defined by Eqs. (7) and (8), corresponding to these three cases. It can be

Table 7 Parameters of the fragility curves

	SMF3				SMF7				SMF13			
	ds ₁	ds ₂	ds ₃	ds ₄	ds ₁	ds ₂	ds ₃	ds ₄	ds ₁	ds ₂	ds ₃	ds ₄
Risk-UE												
Deterministic												
μi (m)	0.084	0.122	0.179	0.329	0.194	0.277	0.389	0.668	0.335	0.470	0.623	0.971
βi	0.340	0.340	0.440	0.570	0.330	0.310	0.390	0.510	0.320	0.270	0.320	0.420
5th percentile												
μi (m)	0.080	0.112	0.148	0.231	0.187	0.260	0.329	0.474	0.311	0.434	0.502	0.629
βi	0.320	0.270	0.320	0.420	0.310	0.250	0.260	0.340	0.290	0.220	0.210	0.210
Median												
μi (m)	0.083	0.119	0.169	0.292	0.192	0.272	0.365	0.580	0.325	0.454	0.587	0.875
βi	0.330	0.310	0.400	0.520	0.330	0.280	0.340	0.440	0.320	0.280	0.290	0.380
95th percentile												
μi (m)	0.087	0.128	0.196	0.382	0.198	0.283	0.399	0.687	0.332	0.473	0.653	1.085
βi	0.340	0.370	0.490	0.630	0.330	0.310	0.390	0.510	0.330	0.290	0.320	0.480
D_{PA}												
Deterministic												
μi (m)	0.145	0.192	0.243	0.305	0.361	0.487	0.599	0.711	0.633	0.797	0.938	1.107
βi	0.260	0.260	0.230	0.170	0.290	0.230	0.170	0.140	0.220	0.190	0.150	0.150
5th percentile												
μi (m)	0.134	0.162	0.195	0.232	0.309	0.381	0.442	0.530	0.566	0.663	0.716	0.787
βi	0.200	0.180	0.150	0.170	0.180	0.160	0.160	0.170	0.140	0.100	0.080	0.080
Median												
μi (m)	0.142	0.185	0.220	0.288	0.341	0.422	0.522	0.639	0.643	0.750	0.868	1.012
βi	0.230	0.220	0.210	0.230	0.190	0.210	0.200	0.180	0.150	0.140	0.140	0.140

Table 7 continued

	SMF3				SMF7				SMF13			
	ds ₁	ds ₂	ds ₃	ds ₄	ds ₁	ds ₂	ds ₃	ds ₄	ds ₁	ds ₂	ds ₃	ds ₄
95th percentile												
μi (m)	0.150	0.208	0.269	0.352	0.382	0.545	0.663	0.766	0.705	0.862	1.001	1.202
βi	0.310	0.280	0.240	0.240	0.330	0.220	0.150	0.130	0.190	0.160	0.150	0.170
DI _{CC}												
Deterministic												
μi (m)	0.148	0.185	0.239	0.313	0.385	0.473	0.581	0.738	0.667	0.786	0.923	1.112
βi	0.190	0.220	0.260	0.270	0.180	0.200	0.210	0.210	0.150	0.150	0.160	0.170
5th percentile												
μi (m)	0.144	0.160	0.190	0.233	0.344	0.390	0.440	0.509	0.610	0.657	0.710	0.784
βi	0.120	0.130	0.160	0.200	0.110	0.120	0.130	0.140	0.070	0.070	0.080	0.090
Median												
μi (m)	0.148	0.180	0.216	0.287	0.362	0.431	0.510	0.633	0.654	0.749	0.862	1.015
βi	0.160	0.190	0.220	0.250	0.160	0.160	0.180	0.200	0.130	0.130	0.140	0.150
95th percentile												
μi (m)	0.153	0.195	0.259	0.359	0.399	0.516	0.645	0.790	0.668	0.822	0.993	1.237
βi	0.220	0.250	0.280	0.300	0.250	0.230	0.200	0.180	0.190	0.190	0.190	0.200

Upper rows correspond to Risk-UE based fragility curves, middle rows correspond to curves based on DI_{PA}, and lower rows correspond to fragility curves based on DI_{CC}. The deterministic case, and the 5th, 50th and 95th percentiles cases are shown. Median fragility curves are shown in Fig. 16

Non-null damage states: ds₁ (slight); ds₂ (moderate); ds₃ (extensive) and ds₄ (complete)

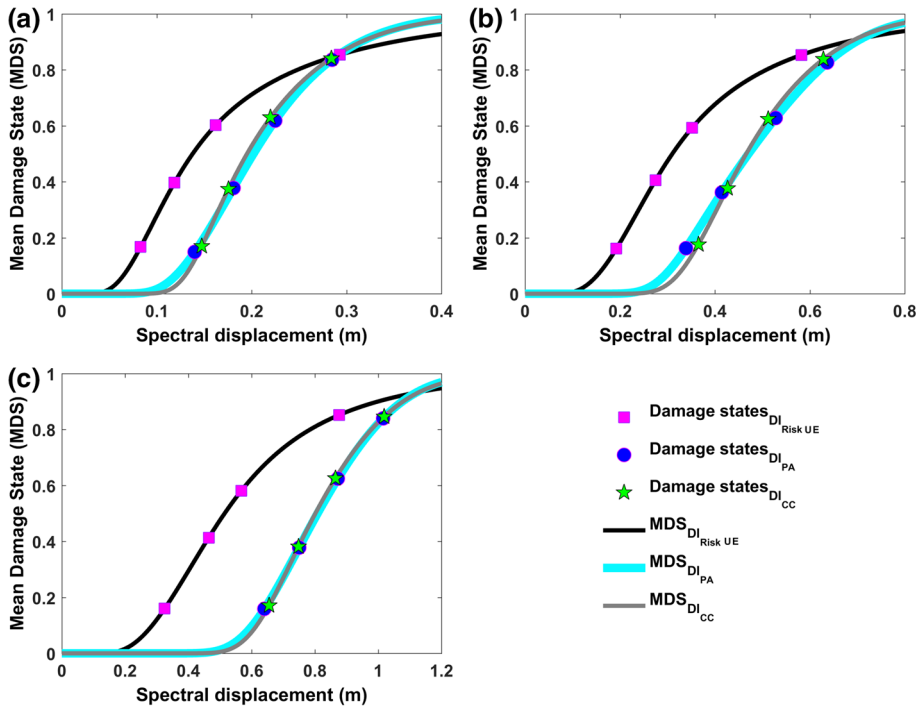


Fig. 17 Comparison of the median MDS functions. **a** SMF 3, **b** SMF 7 and **c** SMF 13

seen that Risk-UE based MDSs overestimate the expected damage. However, in the case of the low-rise building SMF3, the Risk-UE based MDS underestimates the damage above the complete damage state. Disagreements between Risk-UE and DIPA based MDS were also found for reinforced concrete buildings (Pujades et al. 2015). Notwithstanding, the threshold values of displacement adopted for the four damage state limits by Pujades et al. (2015) were based on observations in reinforced concrete buildings (Park et al. 1985, 1987; Cosenza and Manfredi 2000). For easy, the same damage state thresholds to set up fragility and MDS damage curves, based both on DI_{PA} and DI_{CC} damage indices, have been adopted herein for steel buildings; other criteria can be used to define these threshold values, as for instance the damage states based on interstorey drifts proposed in the FEMA (2016) for steel buildings, but in our view, similar results would have been obtained.

8 Overview and discussion

8.1 Overview

In this paper, the parametric model for capacity curves and the new capacity-based damage index and fragility models, recently proposed by Pujades et al. (2015), have been tested and applied to steel buildings. High- (13 storeys), mid- (7 storey) and low-rise (3 storeys) buildings with special moment frames have been evaluated. Also, the seismic response of steel buildings, which are typical of the city of Mexico, has been investigated with deterministic and probabilistic approaches. NLSA and NLIDA are used. The probabilistic

approach uses Monte Carlo simulation and optimization sampling techniques, such as the Latin hypercube technique. Uncertainties in the mechanical properties of buildings and in the seismic actions are considered. Only the strength and ductility of the structural elements are considered as random variables and it is assumed that they follow truncated normal or lognormal probability density distributions. For deterministic analyses, mean values of these distributions are used. Seismic actions are chosen according to the design spectrum foreseen for soft soils in the city of Mexico. Thus, four accelerograms recorded in the study area have been selected, and a spectral matching technique has been applied, so that the response spectra match the design spectrum well. For deterministic analyses, the mean of these four matched accelerograms has been used. For probabilistic analysis, five probabilistic response spectra, with the design spectrum as mean and a predefined SD have been generated. Then, for each generated spectrum, the spectral matching technique is applied to each of the four selected accelerograms, resulting in a suite of 20 accelerograms, whose response spectra have the design spectrum as a mean and the predefined SD.

8.2 Discussion

One of the main purposes of this research has been to check the parametric capacity model and the capacity-based damage index for steel buildings. Actually, Pujades et al. (2015) found a very simple analytical model with five independent parameters, fitting capacity curves well. It was shown how the degradation processes (damaging), which can be isolated in the nonlinear part of the capacity curve, are well represented by a cumulative integral of a cumulative lognormal function. That is by means of only two parameters. The appropriateness of the model may be clearly seen in the first derivatives of the capacity curves. Certainly, the use of a reinforced concrete building to illustrate the model was ad hoc because, at that moment, studies were being carried out on RC buildings. However, the parametric model wants to be valid for any capacity curve. Thus, this research highlights the validity of this fine model, also for steel buildings. Moreover, focusing on the nonlinear part of the capacity curve, in the same paper, Pujades et al. (2015) proposed a new and simple damage index, which, like the Park and Ang damage index, is based on the stiffness degradation and on the energy loss. The parameter α is crucial as it separates the contribution of the stiffness degradation from that of the energy loss. Values around 0.7 are found for this parameter in the very few studies performed up to date. In fact, this value can be taken as a first quick estimate. Finer estimations require NLIDA. Results show that

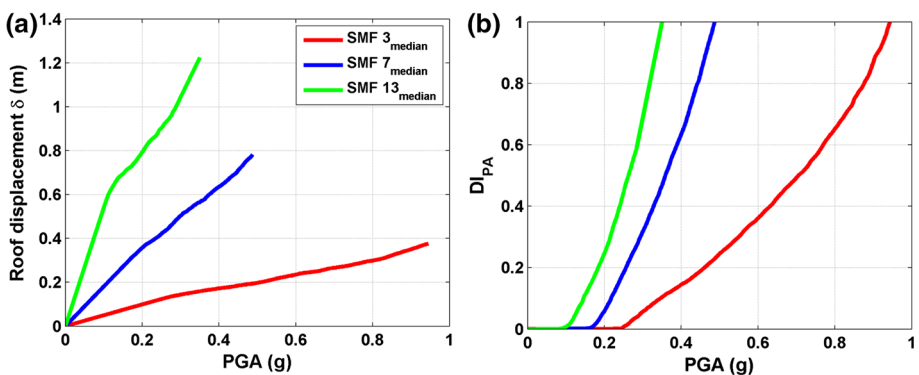


Fig. 18 PGA- δ and PGA- DI_{PA} functions for the three buildings (see explanation in the text)

relatively low variations, around this value of 0.7, are expected, and they are related mainly with the characteristics of the seismic actions. This way, near-fault impulsive strong motions would lead to higher α values. Far-field seismic actions and soft soils would provide long duration seismic actions increasing the contributions to damage of repeated cyclic loads, thus decreasing the α values. Really, future research on more building types, using different seismic actions, can lead to tabulated values of this parameter, facilitating expedite and massive applications of this new damage index. Noticeably, also the fragility curves based on the damage thresholds defined according specific values of this damage index are dependent on the features of the seismic actions, which, on the other hand, would be reasonable.

Additional values of this research are the probabilistic approach adopted, as well as the study of the frame steel buildings located in soft soils of the Mexico City. Concerning the probabilistic approach, our results confirm that the probabilistic approach must be preferred because, due to the nonlinearity of the response of the buildings, the use of deterministic, even conservative, inputs, can lead to biased outputs; besides, probabilistic approach is richer as it allows obtaining and analyse the uncertainties in the response. Uncertainties in the response increase with the severity of the seismic actions. Concerning to the studied buildings, Fig. 18 shows PGA- δ and PGA-DI_{PA} curves obtained with NLIDA.

It can be seen how the high-rise frame steel buildings, located in soft soils in Mexico City, would exhibit no good performance, when subjected to likely seismic actions. Ongoing research (Díaz 2017) shows the adequacy of the use of protecting devices in those buildings. For instance, the use of Buckling Restrained Braced Frames, highly improves their seismic performance. Finally, the use of seismic actions recorded in the study zone, but that, at the same time, are compatible with the design response spectrum also gives reliability to the obtained results.

9 Conclusions

Several relevant conclusions of this research are as follows:

- Because of nonlinearity both of static and dynamic responses, the use of mean, median or characteristic values does not warranty to get mean, median or characteristic responses. This fact highlights the importance of probabilistic approaches in front of the more frequently used deterministic ones. Note that, in our case (see Fig. 13), the use of mean values, both of the seismic actions and strength parameters, leads to unconservative results, which emphasizes, even more, the importance of probabilistic approaches, which should be preferred, as they provide more complete, more valuable and richer information.
- Uncertainties in the response increase with an increase in the severity of the earthquake. The main source of uncertainty in the response is uncertainty in the seismic action, but the influence of uncertainties in the mechanical parameters was also significant, even though it was lower.
- The parametric model for capacity curves, the new damage index based on the secant stiffness degradation and energy loss, and the corresponding fragility model as proposed by Pujades et al. (2015) for reinforced concrete buildings, also provide excellent results for the steel buildings studied herein. This confirms the robustness of the parametric model, the compatibility of the new damage index with the Park and

Ang damage index, and the consistency of the fragility model with previous proposals based on expert judgment.

- Concerning the damage index for the buildings and seismic actions studied in this research, relative contributions to damage due to secant stiffness degradation and those due to energy loss are respectively about 70 and 30%. The contribution to damage of the energy loss is about 10% greater than that obtained by Pujades et al. (2015) for reinforced concrete buildings. This increase is attributed to longer duration of the accelerograms in Mexico City because of the combined effects of large epicentral distances and soft soils. Longer durations entail greater numbers of hysteretic cycles for the same spectral displacements, thus increasing the contribution to damage of energy dissipation.
- For the steel buildings analysed here, static and dynamic analyses provide consistent results. However, differences increase with the height of the buildings; this fact is attributed to the influence of higher modes in the response, which is not captured in the static analysis, as executed here.

The results of this research show that the parametric and damage models proposed by Pujades et al. (2015) for reinforced 2D frame reinforced concrete buildings are also valid for 2D frame steel buildings. Thus, this is a promising new tool that can be useful in rapid damage assessments and, in particular, in probabilistic approaches, as it may allow significant computation time reductions.

Acknowledgements This research was partially funded by the Ministry of Economy and Competitiveness (MINECO) of the Spanish Government and by the European Regional Development Fund (FEDER) of the European Union (UE) through projects referenced as: CGL2011-23621 and CGL2015-65913-P (MINECO/FEDER, UE). The first author holds PhD fellowships from the Universidad Juárez Autónoma de Tabasco (UJAT) and from the ‘Programa de Mejoramiento del Profesorado, México (PROMEP)’. Hidalgo-Leiva DA also holds PhD fellowships from the OAIICE, the Universidad de Costa Rica (UCR), and CONICIT, the Government of Costa Rica.

References

- AISC 341-10 (2010) Seismic provisions for structural steel buildings. American Institute of Steel Construction, Chicago
- ANSI/AISC 358 (2010) Prequalified connections for special and intermediate steel moment frames for seismic applications. American Institute of Steel Construction, Chicago
- Asgarian B, Sadrinezhad A, Alanjari P (2010) Seismic performance evaluation of steel moment resisting frames through incremental dynamic analysis. *J Constr Steel Res* 66(2):178–190
- ATC 40 (1996) Seismic evaluation and retrofit of concrete buildings. Applied Technology Council, Redwood City
- Banon H, Veneziano D (1982) Seismic safety of reinforced concrete members and structures. *Earthq Eng Struct Dyn* 10:179–193
- Barbat AH, Carreño ML, Cardona OD, Marulanda MC (2011) Evaluación holística del riesgo sísmico en zonas urbanas. *Rev int métodos numér cálc diseño ing* 27(1):3–27
- Barbat AH, Vargas YF, Pujades LG, Hurtado JE (2016) Evaluación probabilista del riesgo sísmico de estructuras con base en la degradación de rigidez. *Rev int métodos numér cálc diseño ing* 32(1):39–47
- Barbosa AR, Ribeiro FLA, Neves LAC (2017) Influence of earthquake ground-motion duration on damage estimation: application to steel moment resisting frames. *Earthq Eng Struct Dyn* 46(1):27–49
- Bartlett FM, Dexter RJ, Graesser MD, Jelinek JJ, Schmidt BJ, Galambos TV (2003) Updating standard shape material properties database for design and reliability. *ASCI Eng J* 40(1):1–14
- Bojorquez E, Reyes-Salazar A, Teran-Gilmore A, Ruiz SE (2010) Energy-based damage index for steel structures. *Steel Compos Struct* 10:331–348

- Bozorgnia Y, Bertero V (2001) Improved shaking and damage parameters for post-earthquake applications. In: Proceedings, SMIP01 seminar on utilization of strong-motion data, Los Angeles, pp 1–22
- Bracci JM, Reinhorn AM, Mander JB, Kunnath SK (1989) Deterministic model for seismic damage evaluation of reinforced concrete structures. Technical report NCEER-89-0033, National Center for Earthquake Engineering Research, State University of New York at Buffalo
- Brando G, D'Agostino F, De Matteis G (2015) Seismic performance of MR frames protected by viscous or hysteretic dampers. *Struct Des Tall Spec Build* 24(9):653–671
- Carr AJ (2002) Ruaumoko-inelastic dynamic analysis program. Department of Civil Engineering, University of Canterbury, Christchurch
- Celarec D, Dolšek M (2013) The impact of modelling uncertainties on the seismic performance assessment of reinforced concrete frame buildings. *Eng Struct* 52:340–354
- Cosenza E, Manfredi G (2000) Damage indices and damage measures. *Prog Struct Eng Mater* 2(1):50–59
- Cosenza E, Manfredi G, Ramasco R (1993) The use of damage functional in earthquake engineering: a comparison between different methods. *Earthq Eng Struct Dyn* 22:855–868
- Díaz SA (2017) Análisis estructural sísmico de edificios de acero. Un enfoque probabilista. Ph.D. dissertation. Universitat Politècnica de Catalunya (**in press, in Spanish**)
- Díaz SA, Pujades LG, Barbat AH, Félix JL (2015) Efecto de la direccionalidad en la amenaza sísmica de la Ciudad de México. In: 20th Congreso Nacional de Ingeniería Sísmica. México. Acapulco, Guerrero. ISSN: 2448-5721
- DiPasquale E, Cakmak AS (1990) Seismic damage assessment using linear models. *Soil Dyn Earthq Eng* 9(4):194–215
- FEMA 355C (2000) State of the art report on system performance of steel moment frames subject to earthquake ground shaking. SAC Joint Venture Partnership for the Federal Emergency Management Agency, Washington
- FEMA P-58-1 (2012) Seismic performance assessment of buildings, vols 1, 2. SAC Joint Venture Partnership for the Federal Emergency Management Agency, Washington
- FEMA (2016) Multi-hazard loss estimation methodology. Earthquake model. Hazus[®] MH 2.1. Technical manual. Federal emergency management agency (FEMA). Washington. <https://www.fema.gov/hazus-mh-user-technical-manuals>. Last visited 11 Dec 2016
- FEMA P-1051 (2016) NEHRP recommended seismic provisions: design examples. Federal Emergency Management Agency, Washington
- Fragiadakis M, Vamvatsikos D (2008) Approximate seismic performance uncertainty estimation using static pushover methods. In: Proceedings of the 14WCEE 2008: 14th world conference on earthquake engineering, Beijing, China
- Fragiadakis M, Vamvatsikos D (2010) Fast performance uncertainty estimation via pushover and approximate IDA. *Earthq Eng Struct Dyn* 39:683–703
- Freeman SA (1998) The capacity spectrum method as a tool for seismic design. In: Proceedings of the 11th European conference on earthquake engineering. Paris, France
- Ghosh S, Datta D, Katakhdond AA (2011) Estimation of the Park–Ang damage index for planar multi-storey frames using equivalent single-degree systems. *Eng Struct* 33(9):2509–2524
- Grünthal G (1998) European Macroseismic Scale 1998 EMS-98. Conseil de L'Europe Cahiers du centre Européen de Géodynamique et de Séismologie 15
- Hancock J, Watson-Lamprey J, Abrahamson N, Bommer J, Markatis A, McCoy E, Mendis R (2006) An improved method of matching response spectra of recorded earthquake ground motion using wavelets. *J Earthq Eng* 10(Special Issue 1):67–89
- Ibarra LF, Medina RA, Krawinkler H (2005) Hysteretic models that incorporate strength and stiffness deterioration. *Earthq Eng Struct Dyn* 34(12):1489–1511
- Idota H, Guan L, Yamazaki K (2009) Statistical correlation of steel members for system reliability analysis. In: Proceedings of the 9th international conference on structural safety and reliability (ICOSSAR). Osaka, Japan
- Iman RL (1999) Appendix A: latin hypercube sampling. *Encyclopedia of statistical sciences*, vol 3. Wiley, New York, pp 408–411
- Jaquess TK, Frank KH (1999) Characterization of the material properties of rolled sections. Technical report for SAC Joint Venture, University of Texas. Austin, Texas
- Kamaris GS, Hatzigeorgiou GD, Beskos DE (2013) A new damage index for plane steel frames exhibiting strength and stiffness degradation under seismic motion. *Eng Struct* 46:727–736
- Kazantzi AK, Righiniotis TD, Chryssanthopoulos MK (2008) Fragility and hazard analysis of a welded steel moment resisting frame. *J Earthq Eng* 12:596–615
- Kazantzi AK, Vamvatsikos D, Lignos DG (2014) Seismic performance of a steel moment-resisting frame subject to strength and ductility uncertainty. *Eng Struct* 78:69–77

- Kim S-P, Kurama YC (2008) An alternative pushover analysis procedure to estimate seismic displacement demands. *Eng Struct* 30(12):3793–3807
- Krawinkler H (1978) Shear in beam-column joints in seismic design of steel frames. *Eng J* 15(3):82–91
- Krawinkler H, Zohrei M (1983) Cumulative damage in steel structure subjected to earthquake ground motions. *Comput Struct* 16(1–4):531–541
- Lagomarsino S, Giovinazzi S (2006) Macroseismic and mechanical models for the vulnerability and damage assessment of current buildings. *Bull Earthq Eng* 4(4):415–443
- Lantada N, Pujades LG, Barbat AH (2009) Vulnerability index and capacity spectrum based methods for urban seismic risk evaluation. A comparison. *Nat Hazards* 51:501–524
- Lantada N, Irizarri J, Barbat AH, Goula X, Roca A, Susagna T, Pujades LG (2010) Seismic hazard and risk scenarios for Barcelona, Spain, using the Risk-UE vulnerability index method. *Bull Earthq Eng* 8:201–229
- Levy R, Lavan O (2006) Fully stressed design of passive controllers in framed structures for seismic loadings. *Struct Multidiscip Optim* 32(6):485–498
- Lignos DG, Krawinkler H (2011) Deterioration modeling of steel components in support of collapse prediction of steel moment frames under earthquake loading. *J Struct Eng* 137(11):1291–1302
- Lignos DG, Krawinkler H (2012) Sidesway collapse of deteriorating structural systems under seismic excitations. Technical report no. TB 177, The John A. Blume Earthquake Engineering Center, Stanford University, Stanford, CA
- Lignos DG, Krawinkler H (2013) Development and utilization of structural component databases for performance-based earthquake engineering. *J Struct Eng* 139(8):1382–1394
- Liu XY, Wang YQ, Xiong J, Shi YJ (2017) Investigation on the weld damage behavior of steel beam-to-column connection. *Int J Steel Struct* 17(1):273–289
- McGuire RK (2004) Seismic hazard and risk analysis. Institute Earthquake Engineering Research (EERI), Oakland
- Milutinovic Z, Trendafiloski G (2003) WP04 vulnerability of current buildings RISK-UE project of the EC: an advanced approach to earthquake risk scenarios with applications to different European towns
- Mwafy A, Elnashai A (2001) Static pushover versus dynamic collapse analysis of RC buildings. *Eng Struct* 23(5):407–424
- NTC-DF (2004) Norma técnica complementaria del Distrito Federal. Technical report Gaceta oficial del Distrito Federal, México
- Park YJ (1984) Seismic damage analysis and damage-limiting design of R/C structures. Ph.D. thesis, Department of Civil Engineering, University of Illinois, Urbana, IL
- Park Y-J, Ang AH-S (1985) Mechanistic seismic damage model for reinforced concrete. *ASCE J Struct Eng* ASCE 111:722–739
- Park Y-J, Ang AH-S, Wen YK (1985) Seismic damage analysis of reinforced concrete buildings. *J Struct Eng* ASCE 111:740–757
- Park Y, Ang A-S, Wen Y (1987) Damage-limiting aseismic design of buildings. *Earthq Spectra* 3(1):1–26
- PEER/ATC 72-1 (2010) Modeling and acceptance criteria for seismic design and analysis of tall buildings. Applied Technology Council and Pacific Earthquake Engineering Research Center
- Porter K (2017) A beginner's guide to fragility, vulnerability, and risk. University of Colorado Boulder. <http://spot.colorado.edu/~porterka/Porter-beginners-guide.pdf>. Accessed 6 July 6 2017
- Porter KA, Kennedy RP, Bachman RE (2007) Creating fragility functions for performance-based earthquake engineering. *Earthq Spectra* 23(2):471–489
- Powell GH, Allahabadi R (1988) Seismic damage prediction by deterministic methods: concepts and procedures. *Earthq Eng Struct Dyn* 16(5):719–734
- Pujades LG, Barbat AH, Gonzalez-Drigo R, Avila J, Lagomarsino S (2012) Seismic performance of a block of buildings representative of the typical construction in the Eixample district in Barcelona (Spain). *Bull Earthq Eng* 10:331–349
- Pujades LG, Vargas-Alzate YF, Barbat AH, González-Drigo JR (2015) Parametric model for capacity curves. *Bull Earthq Eng* 13(5):1347–1376
- Rajeev P, Wijesundara KK (2014) Energy-based damage index for concentrically braced steel structure using continuous wavelet transform. *J Constr Steel Res* 103(1):241–250
- Roufaiel MSL, Meyer C (1987) Analytical modeling of hysteretic behavior of R/C frames. *J Struct Eng* ASCE 113(3):429–457
- SAC (1996) Analytical and field investigations of buildings affected by the Northridge earthquake. Report no. SAC-95-04, prepared by SAC Joint Venture, a partnership of SEAOC, ATC and CUREE
- Sallaberry CJ, Helton JC, Hora SC (2008) Extension of Latin hypercube samples with correlated variables. *Reliab Eng Syst Saf* 93(7):1047–1059

- Satyarno I (2000) Adaptive pushover analysis for the seismic assessment of older reinforced concrete buildings. Doctoral thesis, Department of Civil Engineering, University of Canterbury
- Schmidt BJ, Bartlett FM (2002) Review of resistance factor for steel: data collection. *Can J Civ Eng* 29:98–108
- Vamvatsikos D (2014) Seismic performance uncertainty estimation via IDA with progressive accelerogram-wise latin hypercube sampling. *J Struct Eng* 140(8):A4014015-1-10
- Vamvatsikos D, Cornell CA (2002) Incremental dynamic analysis. *Earthq Eng Struct Dyn* 31(3):491–514
- Vargas YF, Pujades LG, Barbat AH, Hurtado JE (2013) Capacity, fragility and damage in reinforced concrete buildings: a probabilistic approach. *Bull Earthq Eng* 11(6):2007–2032
- Wen YK, Ellingwood BR, Veneziano D, Bracci J (2003) Uncertainty modeling in earthquake engineering. MAE Center Project FD-2 Report
- Zhou Z, Qian J, Huang W (2016) Application of modified Park–Ang damage model to steel members. *J Build Struct* 37(1):448–454